ANALYSIS OF INTEGRATED SPACECRAFT PERFORMANCE USING A ROTATING DETONATION ROCKET ENGINE

M.J. Cooper, D.E. Paxson, and H.D. Perkins
NASA Glenn Research Center
Cleveland, Ohio

J.E. Fittje
Science Application International Corporation
Fairfax, Virginia

ABSTRACT

For spacecraft with especially stringent mass fraction constraints, the use of a rotating detonation rocket engine (RDRE) may yield potentially significant system mass savings. The pressure gain combustion inherent to RDREs provides higher thrust than traditional rocket engines for a given supply pressure and throat area. This opens multiple avenues for reducing system mass via higher specific impulse, reduced gravity losses, and reduced feed pressures.

To highlight the potentially weight-saving characteristics of RDRE systems, the integrated performance of representative spacecraft designs using either a conventional rocket engine or an RDRE was assessed. This paper details the assumptions, methods, and results of this trade study. Two representative spacecraft were assessed. The first is a Liquid Mars Ascent Vehicle (MAV). This spacecraft was designed by NASA in 2011 for the Mars Sample Return Campaign but was not selected for flight due in part to it exceeding the mass requirements by 119 lbm. The second is MIURA-1, a kerolox sounding rocket developed by Payload Aerospace S.L..

The Liquid MAV assessment showed that an RDRE powered design met the mass requirements with a total vehicle mass 46 lbm below the limit. The MIURA-1 assessment showed that wall heat transfer and regenerative cooling are significant challenges for kerolox RDREs, but these challenges may be mitigated by reducing mixture ratio and using both propellants to cool the chamber. The assessment showed that an RDRE powered sounding rocket could achieve 12% more microgravity time than a conventional sounding rocket with the same payload and total vehicle mass. Alternately, if the payload mass and target apogee are held constant, then an RDRE powered sounding rocket can be 8% shorter and 11% lighter than a conventional sounding rocket. These results suggest that the advent of RDREs for in-space propulsion may unlock new missions for which conventional propulsion is not feasible.

INTRODUCTION

In a conventional rocket engine, propellants are injected into a chamber at high pressure, undergo combustion at constant pressure via deflagration, and are expelled through a nozzle to produce thrust. Although there is no one parameter governing rocket engine performance, this chamber pressure has a significant impact on a system's performance. The engine thrust will typically increase with chamber pressure. The chamber pressure during engine operation is constant at a given design point in a conventional rocket engine. Thus, increasing chamber pressure can only be achieved by increasing the manifold pressure supplying the chamber. This incurs a mass penalty.

An alternative method for increasing chamber pressure exists via pressure gain combustion (PGC) [1]. PGC differs from constant pressure combustion by, as the name implies, increasing the chamber pressure during the combustion process. The most basic form of a PGC cycle is one where combustion occurs within a constant volume. This results in a higher average chamber pressure without paying the mass penalty of increasing manifold pressure. The rocket propulsion community has indicated considerable interest in PGC technology [1], in particular the rotating detonation rocket engine (RDRE). In an RDRE, the combustion chamber is an annulus with a narrow detonation channel. A supersonic detonation wave travels circumferentially around this channel. Propellants are injected into this chamber axially to form a detonable

mixture. When the detonation wave passes through this mixture, the coupled shock and combustion wave act similarly to a constant volume process, substantially raising both the temperature and total pressure. The exhaust products are then expelled through a nozzle. Meanwhile, the detonation wave continues its journey around the annulus, propelled by the combustion reaction as it ingests fresh propellant. A simplified diagram is provided in Figure 1. The shock generated by the detonation reaction is expected to produce excellent propellant mixing characteristics, thus giving high combustion efficiency. An RDRE can theoretically achieve the same thrust as a conventional rocket engine while being smaller, lighter, and requiring a lower propellant supply pressure.

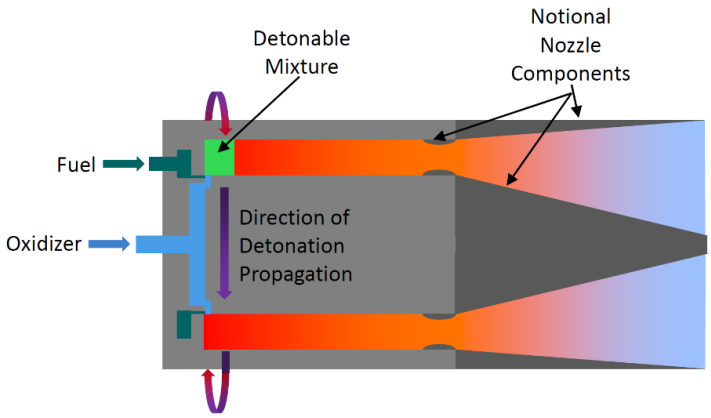

Figure 1: Simplified diagram of RDRE concept [1]

NASA requires efficient and high-performance propulsion systems for its sustainable Moon to Mars architecture. The mass allowances for lunar and Martian missions are especially stringent. Some missions may require propulsion system performance that exceeds currently available technology. Thus, the RDRE is a potentially game-changing development for NASA's exploration goals. Test programs underway at Marshall Space Flight Center (MSFC) have completed long duration RDRE hot fires lasting up to 133 seconds [2]. In this paper, the integrated performance of RDRE-powered spacecraft is assessed via system trades. The performance of two spacecraft will be evaluated, trading their conventional propulsion system for an RDRE. The performance gains and losses caused by this trade will be discussed in detail. The first spacecraft that will be discussed is the Liquid Mars Ascent Vehicle (L-MAV), a NASA in-house design for carrying soil samples to orbit from the Martian surface [3]. The second spacecraft that will be discussed is MIURA-1, a suborbital sounding rocket developed by Payload Aerospace S.L. (PLD Space) [4].

LIQUID MARS ASCENT VEHICLE

The L-MAV was designed by the Collaborative Modeling for Parametric Assessment of Space Systems (COMPASS) group at NASA. The design was intended for the Mars Sample Return Campaign (MSRC). The required wet mass was 637 lbm; however, the conventional bipropellant rocket powered design had a final wet mass of 756 lbm. Thus, the vehicle was 119 lbm overweight, and alternate strategies were pursued for the MSRC. For this reason, the L-MAV is an attractive candidate for an RDRE trade, where utilizing an RDRE could result in significant mass savings. Additionally, since the L-MAV is a NASA design, all design information is available in detail. A simplified model of the L-MAV is provided in Figure 2.

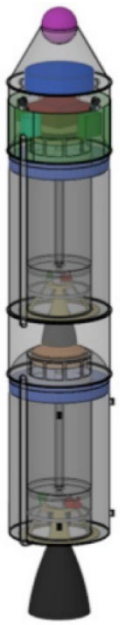

Figure 2: Simplified L-MAV design model [3]

The L-MAV design uses monomethyl hydrazine (MMH) for fuel and a mixture of 75% nitrogen tetroxide plus 25% nitric oxide (MON-25) for oxidizer. The propellants are stored in coaxial piston tanks. A solid propellant gas generator system is used to apply pressure to the piston and drive propellant out of the tank. The tanks are constructed of laminated carbon fiber-reinforced polymer matrix composite, with aluminum endcaps. The tanks were designed with a safety factor of 1.5. For cost-savings, the 1st stage and 2nd stage have identical tanks. The engine is a single use ablatively cooled design. An overview of the L-MAV design parameters is provided in Table 1. All dry masses are provided with an added 30% mass growth allowance per NASA and AIAA guidelines.

The ground rules for this system trade are:

1. The design shall be optimized for minimum mass. For fair comparison, this optimization will be performed for the conventionally powered L-MAV, and an RDRE powered L-MAV. The results will be compared to evaluate how much mass reduction can be directly attributed to the RDRE.
2. Engine envelope must not exceed the original design's engine envelope.
3. The 1st and 2nd stages shall use identical propellant tank dimensions, pressures, and propellant loads, as in the original design.
4. Mixture ratio, tank diameter, injector pressure drop, and feed system pressure drop are held constant at the baseline values.
5. Tank pressure, tank length, tank mass, engine mass, pressurant mass, and propellant mass are allowed to vary.
6. Minimum RDRE mean chamber diameter of 1 inch.

Several models are used to assess the L-MAV performance. These models are described below .

Table 1: Design information used for Liquid Mars Ascent Vehicle trade study

Parameter	Stage 1	Stage 2
Thrust	900 lbf	300 lbf
Specific Impulse	325 sec	325 sec
Mixture Ratio	2.2 O/F	2.2 O/F
Nozzle Area Ratio	150	150
Throat Diameter	0.86"	0.50"
Chamber Pressure	800 psia	800 psia
Tank Pressure	1300 psia	1300 psia
Injector ΔP	400 psid	400 psid
Feed System ΔP	100 psid	100 psid
Engine Envelope	18.6" long, 10.7" dia.	9.9" long, 10.7" dia.
Tank Mass	35.9 lbm	35.7 lbm
Engine Mass	9.9 lbm	6.2 lbm
Pressurant Mass	7.9 lbm	10.1 lbm
Other Mass (i.e. avionics, payload)	29.3 lbm	116.2 lbm
Usable Propellant	247.6 lbm	246.0 lbm
Unusable Propellant	2.6 lbm	8.6 lbm
Total Mass	333.3 lbm	422.8 lbm

CONVENTIONAL ROCKET PERFORMANCE MODEL

The L-MAV conventional rocket engine's performance is modeled using Chemical Equilibrium with Applications (CEA) [6]. The combustion heat released per mass of reactant (heat of reaction) is calculated using CEA's constant-enthalpy and constant-temperature reaction models, which assume complete combustion. This value is then multiplied by a thermal efficiency and added to the reactant mixture enthalpy to get an effective chamber enthalpy. The thermal efficiency is analogous to combustion efficiency, but it also accounts for heat losses to the ablatively cooled chamber walls. CEA's rocket model can then be used with this chamber enthalpy to model the rocket performance. The chamber pressure, mixture ratio, and nozzle area ratio are input to the model. The Martian atmosphere's effect on engine performance is neglected, vacuum operation is assumed. The engine specific impulse and characteristic velocity are calculated using a weighted average of the CEA results, with 1/3 weight applied to the result where flow composition is assumed frozen at the throat, and 2/3 weight is applied to the result where flow composition is assumed to be at equilibrium throughout the nozzle.

The engine's thermal efficiency is assumed to be 80%, as this results in a 325 second vacuum specific impulse at a 150:1 nozzle area ratio. The model predicts that the characteristic velocity at this condition is 5398 ft/sec. Note that, since CEA does not model chamber heat losses, the combustion efficiency used here is not a true combustion efficiency. Rather, it is a measure of how much available reaction energy is spent to produce thrust. Using the CEA results for specific impulse and characteristic velocity, the thrust is calculated using Eqn 1.

$$F = \frac{g_c P_c A_t I_{sp}}{C^*} \qquad \textit{Eqn 1}$$

Where:

F = Thrust
g_c = Unit conversion factor for English units (32.174 lbm-ft/lbf/s^2)
P_c = Chamber pressure
A_t = Throat area
I_{sp} = Specific impulse
C^* = Characteristic velocity

RDRE PERFORMANCE MODEL

RDRE performance is modeled using a reduced-order cycle code, developed in-house at Glenn Research Center [7]. A public version of this code is maintained by the authors of this study and is available on the NASA Software Catalog (https://software.nasa.gov/software/LEW-20423-1). This cycle code has been previously reported in detail. A brief description is provided here.

The cycle code simplifies the exhaust gas mixture into a calorically perfect ideal gas. The reactant mixture's specific gas constant (*R)* is used. The specific heat ratio (γ) is determined by first simulating an ideal Atkinson cycle using thermodynamic data from CEA. In this CEA calculation, the specific heat ratio is allowed to vary. Then, an ideal Atkinson cycle is simulated using isentropic flow equations with constant specific heat ratio. An iterative procedure is used to calculate the specific heat ratio that results in the same specific impulse between the two methods. The heat of reaction is calculated using the same method described for the conventional rocket performance model.

A radial slice of the RDRE chamber is simulated as a lumped volume. When the detonation wave passes over this slice, the reaction heat is released instantaneously. A constant volume calculation determines the post-detonation total pressure and total temperature in the chamber. A blowdown process is then simulated by numerically integrating the time dependent continuity and energy equations using a two-step Runge-Kutta method. A wall heat transfer model estimates the thermal energy loss to the chamber walls. The chamber refill process is simulated based on user-input information on the manifold pressure and the injector pressure loss. The manifold pressure minus the injector pressure loss is referred to as the initial pressure. Further detail is provided in Section II of [7].

The RDRE chamber dimensions are described using three parameters. Hub-to-tip ratio is the ratio of the annulus inner diameter over the annulus outer diameter (Eqn 2). Chamber aspect ratio is the chamber length divided by the channel hydraulic diameter, namely, 2x the detonation channel width (Eqn 3). Mean diameter is the average of the annulus inner and outer diameters (Eqn 4). The limits of hub-to-tip ratio and chamber aspect ratio are not well understood for RDREs. Lower hub-to-tip ratios increase the throat area, enabling more thrust for a given initial pressure and mean diameter. Lower aspect ratios reduce the available surface area for heat losses for a given mean diameter. [22] provides an overview of experimental liquid bipropellant RDE configurations, including chamber dimensions, that have been ran successfully. For the L-MAV study, the hub-to-tip ratio is assumed to be 0.8, and the aspect ratio is assumed to be 5.

$$[h/t]_{chamber} = \frac{D_{inner}}{D_{outer}} \qquad \textit{Eqn 2}$$

$$AR_{chamber} = \frac{L_{chamber}}{D_{outer} - D_{inner}} \qquad \textit{Eqn 3}$$

$$D_{mean} = \frac{1}{2}(D_{inner} + D_{outer}) \qquad \textit{Eqn 4}$$

Table 2: RDRE cycle code settings for L-MAV trade study

RDRE Cycle Code Input	Value Used
Specific Heat Ratio	1.2360
Heat of Reaction	9939 BTU/lbm
Specific Gas Constant	61 ft-lbf/lbm/°R
Hub-to-Tip Ratio	0.80
Chamber Aspect Ratio	5
Wall Temperature	2500 °R
Throat Area Ratio	0.80
Exhaust Prandtl Number	0.7
Combustion Efficiency	97%
Initial Temperature	540 °R

Where:
h/t = Hub-to-tip ratio
D = Diameter
AR = Aspect Ratio
L = Length

The conventional L-MAV system is an expendable, ablatively cooled engine. The RDRE system is assumed to be the same. Based on prior experience with passively cooled in-space thrusters, the wall material is assumed to be a C-103 alloy at 2500 °R with material properties in Table 4. A nozzle heat transfer model, developed for the MIURA-1 trade study, showed that nozzle heat losses account for 5% of the total exhaust heat loss for the L-MAV. Chamber heat losses account for the remaining 95%. As such, nozzle heat losses are neglected for the L-MAV study. The cycle code settings used for the L-MAV trade study are provided in Table 2.

NOZZLE GEOMETRY MODEL

Since the engine envelope must not exceed the original design's engine envelope, an accurate estimate of the nozzle contour is required. The converging section of the nozzle is assumed to follow a 30° wall angle. The diverging section of the nozzle is a parabolic Rao nozzle with a specified length, throat wall angle, and exit wall angle [5]. The diverging section length is calculated by initially setting the wall angle to 15°. The length required to achieve the desired nozzle area ratio is calculated. Then, the true nozzle's diverging section length is set equal to 80% of this value. The throat wall angle is set equal to 1/3 the Prandtl-Meyer angle of the nozzle exit Mach number. The exit wall angle is set according to Eqn 5.

$$\theta_{exit} = \frac{1}{2} * \sin^{-1}\left(\frac{2}{\gamma M_e^2}\cot\left(\sin^{-1}\frac{1}{M_e}\right)\right) \qquad \textit{Eqn 5}$$

Where:
θ_{exit} = Exit wall angle
M_e = Exit Mach number

Table 3: L-MAV nozzle model validation

Nozzle Length	Stage 1	Stage 2
Predicted	14.4"	8.3"
Actual	14.1"	7.8"
Error	+2.1%	+6.4%

A parabolic contour is fit to the required length, throat wall angle, and exit wall angle. The nozzle geometry model was run at the L-MAV design point. An excellent agreement between the model length and actual length is shown in Table 3. For a given L-MAV configuration, the maximum possible nozzle area ratio that can fit within the engine envelope is used. This maximizes specific impulse. An example of the nozzle geometry model output is provided in Figure 4 and Figure 5. Note that the combustion chamber geometry is a user-input.

MASS ESTIMATE MODEL

The chamber and nozzle mass are calculated by integrating the wall thickness over the engine contour length. The required wall thickness is calculated using the circumferentially averaged pressure at each nozzle station, based on the isentropic nozzle equations and the chamber stagnation state. Note that for a conventional rocket engine, a circumferential average does not need to be calculated as the pressure at a given nozzle station is constant in time and space. For the outer body, a hoop stress calculation determines the wall thickness (Eqn 6). For the inner body, a buckling calculation determines the wall thickness (Eqn 7) [8].

$$\sigma_{hoop} = P_x * \frac{D_{outer,x}^2 + D_{outer,x}t_{outer,x} + t_{outer,x}^2}{D_{outer,x}t_{outer,x} + t_{outer,x}^2} = \frac{\sigma_{yield}}{FS} \qquad \textit{Eqn 6}$$

$$P_{buckle} = 0.35 * \frac{E}{1-\nu^2}\left(\frac{2 * t_{inner,x}}{D_{inner,x}}\right)^2 = P_x * FS \quad \text{Eqn 7}$$

Where:

σ = Wall stress
P_x = Pressure at an axial station
D_x = Diameter at an axial station
t_x = Wall thickness at an axial station
FS = Factor of safety
E = Young's Modulus
ν = Poisson's ratio

Table 4: Engine material properties used for L-MAV trade study [9]

Assumed Wall Material Properties	Value Used
Elastic modulus	24,500 ksi
Yield strength	18,000 psi
Poisson's ratio	0.33
Density	0.320 lbm/in^3
Safety factor	1.5

Table 5: Baseline engine mass values used for L-MAV trade study [3]

Baseline Engine Mass	Stage 1	Stage 2
Chamber & nozzle mass, predicted	2.5 lbm	1.1 lbm
Total mass, actual	9.9 lbm	6.2 lbm
Assumed component mass	7.4 lbm	5.1 lbm

Scaling laws were developed for the remaining engine mass – that is, the injector head mass, valve mass, ablator mass, and any other components not captured by the nozzle and chamber mass. The chamber and nozzle masses were estimated for the baseline L-MAV using a minimum allowable wall thickness of 0.001" and a safety factor of 1.5. Using a very small minimum allowable wall thickness and safety factor produces an underestimate for the nozzle and chamber mass. This is done to make the assumed component mass conservatively high. The estimated chamber and nozzle mass were subtracted from the baseline L-MAV engine mass to produce an assumed component mass. The resulting mass breakdown is provided in Table 5.

Since the engine is ablatively cooled, the ablator mass is assumed to scale linearly with the mass-averaged chamber temperature. It should be noted that this is a very blunt estimate of the impact from exhaust heat transfer – for the L-MAV study, understanding the impact of heat transfer is low-priority due to its ablatively cooled expendable system. For this reason, the MIURA study investigates heat transfer effects in greater detail. The resulting scaling law for Stage 1 engine mass is listed in Eqn 8. The scaling law for Stage 2 engine mass is listed in Eqn 9.

$$m_{engine,1} = 7.4[lbm] * \left(\left(\frac{T_{chamber,mass\ avg,1}}{5600[°R]}\right) + \left(\frac{\dot{m}_1}{2.8\left[\frac{lbm}{sec}\right]}\right)\right) + m_{chamber,1} + m_{nozzle,1} \quad \text{Eqn 8}$$

$$m_{engine,2} = 5.1[lbm] * \left(\left(\frac{T_{chamber,mass\ avg,2}}{5600[°R]}\right) + \left(\frac{\dot{m}_2}{0.9\left[\frac{lbm}{sec}\right]}\right)\right) + m_{chamber,2} + m_{nozzle,2} \quad \text{Eqn 9}$$

Since all L-MAV design information is known, the propellant tank mass can be estimated very accurately. Since the propellant tank diameter is held constant at the baseline value, the tank barrel length scales linearly with tank propellant load. The barrel thickness scales linearly with pressure. Some tank component masses are independent of pressure – i.e. pistons and mechanisms. The resulting scaling law for propellant tank pressure is listed in Eqn 10.

$$m_{tank} = 28.7[lbm] * \left(\frac{m_{prop}[lbm]}{252.4[lbm]}\right)\left(\frac{P_{tank}}{1300[psia]}\right) + 3.4[lbm] \quad \text{Eqn 10}$$

The Stage 1 and Stage 2 propellant tank pressurant mass is estimated using a similar method in Eqn 11 and Eqn 12, respectively.

$$m_{pressurant,1} = 7.9[lbm] * \left(\frac{m_{prop}[lbm]}{252.4[lbm]}\right)\left(\frac{P_{tank}}{1300[psia]}\right) \quad \textit{Eqn 11}$$

$$m_{pressurant,2} = 10.1[lbm] * \left(\frac{m_{prop}[lbm]}{252.4[lbm]}\right)\left(\frac{P_{tank}}{1300[psia]}\right) \quad \textit{Eqn 12}$$

Table 6: L-MAV baseline propellant tank properties [3]

Baseline Tank Properties	Value
Barrel mass	28.7 lbm
Component mass	3.3 lbm
Design pressure	1,300 psia
Design propellant load	252.4 lbm

TRAJECTORY MODEL

At the design point, the required delta-V to achieve the desired orbit is 3907 m/s. A 1.5% flight performance reserve is bookkept for delta-V, increasing the design delta-V to 3966 m/s. A COMPASS trajectory analysis showed that over a limited range of thrust-to-weight ratios (TWR) for each stage, the required delta-V is a linear function of TWR. This linear relationship holds for Stage 1 TWR from 3.1 to 6.4, and Stage 2 TWR from 1.8 to 5.5. The lower TWR limit for this relationship is the design point for the conventional L-MAV. This produces a simple model for the delta-V required as a function of Stage 1 TWR and Stage 2 TWR in Eqn 13. This model includes the effect of Mars atmospheric drag.

$$\Delta V_{req} = 1.015 * \left(3907\left[\frac{m}{s}\right] - 31.8\left[\frac{m}{s}\right] * (TWR_1 - 3.13) - 53.9\left[\frac{m}{s}\right](TWR_2 - 1.85)\right) \quad \textit{Eqn 13}$$

Designs with TWR outside of this range are out of the scope of this trade study. Note that TWR is calculated using Mars surface gravity. The delta-V delivered by the L-MAV is calculated using the rocket equation. The wet and dry masses for each stage are calculated using the mass estimate models (Eqn 14-Eqn 17).

$$m_{dry,2} = m_{tank} + m_{pressurant,2} + m_{engine,2} + 124.8[lbm] \quad \textit{Eqn 14}$$

$$m_{wet,2} = m_{dry,2} + (m_{prop} - 8.6[lbm]) \quad \textit{Eqn 15}$$

$$m_{dry,1} = m_{wet,2} + m_{tank} + m_{pressurant,1} + m_{engine,1} + 31.9[lbm] \quad \textit{Eqn 16}$$

$$m_{wet,1} = m_{dry,1} + (m_{prop} - 2.6[lbm]) \quad \textit{Eqn 17}$$

Note that the mass and delta-V equations are coupled with the scaling laws and performance models described above. An iterative procedure is used to calculate the gross liftoff mass (GLOM) for any particular L-MAV configuration.

L-MAV TRADE STUDY RESULTS

Per the system trade ground rules, the conventionally powered L-MAV system was optimized for minimum GLOM. A parametric sweep was performed on all parameters in the trade space. The tank pressure and throat diameters are the independent variables. If these values are known, then all other parameters can be calculated using the models described above. The minimum GLOM achieved for each tank pressure evaluated is shown in Figure 3. The results show that the optimal propellant tank pressure for a conventionally powered L-MAV is 740 psia. The GLOM as a function of throat diameter at 740 psia tank pressure is shown in Figure 17 in the appendix. At the optimal point, the 1st stage TWR is maximized to minimize gravity losses. This requires the largest possible throat diameter, which reduces the nozzle area ratio. The 2nd stage uses the smallest possible throat diameter to maximize the nozzle area ratio. Further optimization may be possible if the allowable TWR range is expanded, but this is outside the scope of this trade study. The optimal point GLOM is 643 lbm for the conventionally powered L-MAV. This is 6 lbm greater than the required GLOM of 637 lbm. Thus, even after optimizing for minimum mass, **a conventionally powered L-MAV cannot meet the design requirements.**

Next, the RDRE powered L-MAV system was optimized for minimum GLOM. A parametric sweep was once again performed on all parameters in the trade space. The tank pressure and mean chamber diameters are the independent variables. The minimum GLOM achieved for each tank pressure evaluated is shown in Figure 3. The results show that the optimal propellant tank pressure for an RDRE powered L-MAV is 680 psia. The GLOM as a function of RDRE mean chamber diameter at 680 psia tank pressure is shown in Figure 18 in the appendix. As was the case for the conventional L-MAV, the optimal point has the 1st stage TWR maximized to minimize gravity losses, and the 2nd stage has the nozzle area ratio maximized to maximize specific impulse. The optimal point GLOM is 591 lbm for the RDRE powered L-MAV. This is 46 lbm below the required GLOM of 637 lbm. Thus, **an RDRE powered L-MAV meets the design requirements**.

Table 7: Model outputs for engine performance in optimized RDRE L-MAV. Engine geometry is shown in Figure 3 and Figure 4.

Parameter	Stage 1	Stage 2
Thrust	1,450 lbf	230 lbf
Initial pressure	180 psia	180 psia
Nozzle area ratio	41.0	113.7
Mean diameter	2.8”	1.1”
Specific impulse	321.8 sec	330.4 sec
Wall heat loss	1,200 BTU/sec	219 BTU/sec
Wall heat loss as percent of total reaction heat	8.8%	10.3%
Combustion chamber channel width	0.31”	0.12”
Combustion chamber length	3.1”	1.2”
Detonation frequency	12,400 Hz	31,500 Hz

The optimization results are compared in Table 8. Increasing TWR reduced the required ΔV for both the optimized L-MAVs. Therefore, mass savings due to increased thrust cannot be solely attributed to the RDRE. However, the propellant tank mass is significantly reduced for the RDRE optimized L-Mav. Using an RDRE reduced the propellant tank mass significantly, due to the lower tank pressures enabled by pressure gain combustion. Therefore, mass savings due to reduced tank pressure can be attributed to the RDRE. The lower inert mass reduced the amount of propellant needed to meet the ΔV requirement. The RDRE geometry required a lower nozzle area ratio to fit within the engine envelope. This reduced specific impulse compared to the baseline L-MAV; however, this was balanced by the RDRE’s increased combustion efficiency. The RDRE powered L-MAV achieved a 165 lbm mass reduction over the baseline design. Based on the optimization comparison, 52 lbm of this mass reduction can be directly attributed to the usage of an RDRE.

Table 8: Comparison of different L-MAV configurations

Parameter	Baseline L-MAV	Optimized Conventional L-MAV	Optimized RDRE L-MAV
Required ΔV	13,011 ft/sec	12,692 ft/sec	12,678 ft/sec
Total propellant load	504.8 lbm	432.5 lbm	389.0 lbm
Total tank mass (incl. pressurant)	89.7 lbm	43.7 lbm	37.3 lbm
Total engine mass	16.1 lbm	21.7 lbm	19.5 lbm
Gross liftoff mass	756.2 lbm	643.4 lbm	591.3 lbm
Mass margin	-119.2 lbm	-6.4 lbm	+45.7 lbm

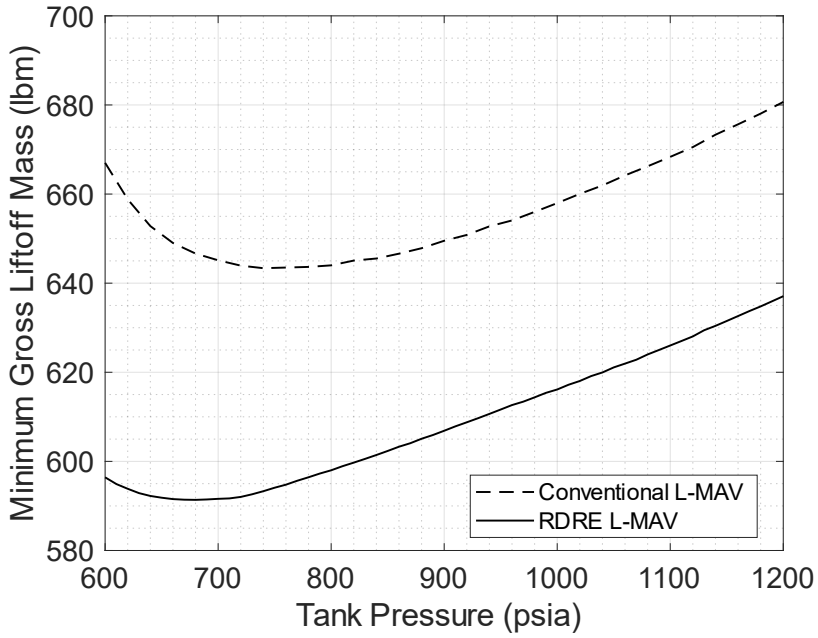

Figure 3: Optimized GLOM as a function of tank pressure for a conventional or RDRE powered L-MAV

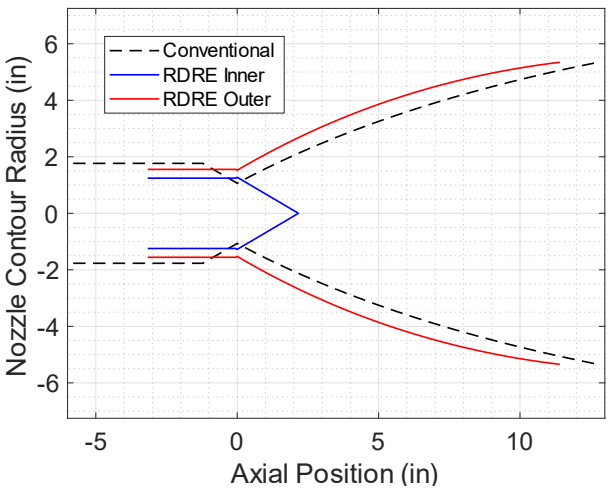

Figure 4: Optimized L-MAV stage 1 engine geometry

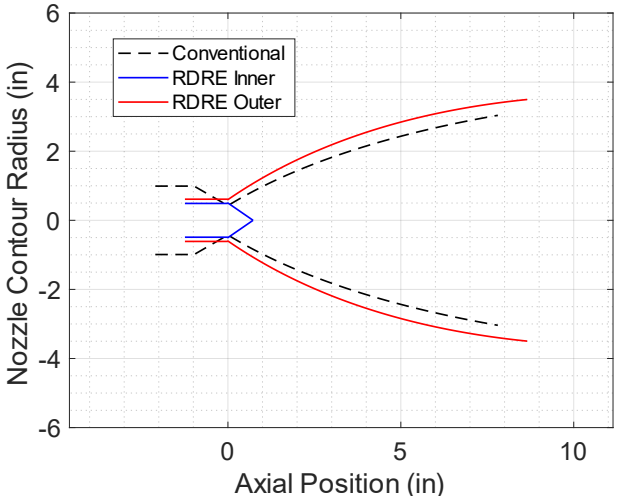

Figure 5: Optimized L-MAV stage 2 engine geometry

MIURA-1

MIURA-1 is a suborbital sounding rocket developed by Payload Aerospace S.L. (PLD Space). MIURA-1 is a single stage pressure-fed design powered by kerosene and liquid oxygen. Pressure is provided by helium stored in a composite overwrapped pressure vessel (COPV). It is intended to carry up to 200 lbm of science payload on a suborbital trajectory. PLD space performed a test flight on October 7, 2023 which the company stated met all test objectives. MIURA-1 exhibits desirable characteristics for an RDRE trade. For one, its conventional TEPREL-B propulsion system puts out 6,800 lbf of sea level thrust, which is a similar thrust class to the RDRE demonstrators run on test stands to date [2]. Unlike the L-MAV, MIURA-1 has been built and flown, and is designed to be recovered and reused. MIURA-1 lifts off from Earth sea level under ambient atmospheric conditions, meaning the pressure gain combustion achieved by an RDE provides a more potent efficiency gain compared to vacuum conditions. Most significantly for this study, the conventional rocket engine (TEPREL-B) is regeneratively cooled. This provides an excellent opportunity to evaluate the integrated performance of a regeneratively cooled kerolox RDRE.

Figure 6: MIURA-1 [4]

An overview of known MIURA-1 design information is provided below. All information in Table 9 is provided by PLD Space in their public materials [4]. Information in Table 10 is calculated from public information. The propellant flow rates are calculated from the reported thrust, specific impulse, and mixture ratio. The flow rates are multiplied by the reported burn time to calculate the usable propellant load. The supply delta-P describes the pressure drop from the propellant tanks to the combustion chamber. This delta-P includes all feed system and injector pressure losses.

The ground rules for this system trade are as follows:

1. RDRE thrust shall be held constant at the 6,800 lbf baseline sea level value.
2. Tank diameter, injector pressure drop, and feed system pressure drop are held constant at the baseline values.
3. Tank pressure, tank length, tank mass, engine mass, pressurant mass, and propellant mass are allowed to vary.

Table 9: Publicly available baseline MIURA-1 design information

Parameter	Known Value
Thrust (sea level)	6,800 lbf
Specific impulse	240 sec
Mixture ratio	2.35 O/F
Engine burn time	122 sec
Chamber pressure	320 psia
Diameter	27.5”
Total wet mass	5,620 lbm
Fuel tank pressure	390 psia
Fuel tank volume	600 L
Oxid tank pressure	520 psia
Oxid tank volume	1000 L
Oxid tank temperature	164 °R
Helium COPV volume	260 L
Helium COPV pressure	6,000 psia

Table 10: Additional MIURA-1 information, calculated from Table 9

Parameter	Calculated Value
Fuel Flow Rate	8.44 lbm/sec
Usable Fuel Load	1,030 lbm
Fuel Supply ΔP	70 psid
Oxid Flow Rate	19.8 lbm/sec
Usable Oxid Load	2,420 lbm
Oxid Supply ΔP	200 psid
Ullage Volume Fraction	4%
Total Inert Mass (excluding payload)	1,950 lbm
Total Usable Propellant	3,450 lbm

REGENERATIVE COOLING MODEL

A regenerative cooling jacket model was developed for trading an RDRE with the TEPREL-B rocket engine. The regen jacket model solves for the coolant temperature rise and pressure drop through rectangular cooling channels in the combustion chamber and nozzle walls. The model simultaneously solves for the exhaust temperature and pressure decrease through the combustion chamber and nozzle. The performance of regeneratively cooled RDREs is the primary focus of the MIURA-1 trade, therefore the regenerative cooling model is necessarily complex. An overview is provided here, but it is not exhaustive of every detail.

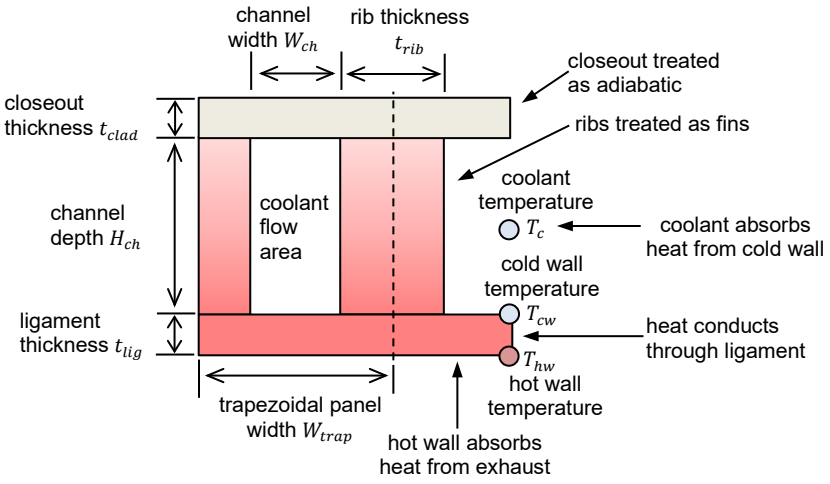

Figure 7: Geometry diagram showing a coolant channel cross section for the regenerative cooling jacket model

The exhaust and coolant flows are modeled as 1-dimensional by marching along the engine axis and solving for temperature and pressure changes. The combustion chamber and nozzle are discretized axially into stations. The curved walls are simplified into multiple flat, trapezoidal panels. These panels are drawn in-between the axial stations, and are centered on the cooling channels, i.e. a jacket with 4 cooling channels will have 4 panels per station, giving a square cross-section. The nozzle geometry model previously described for the L-MAV is used to calculate the nozzle contour. The hot wall temperature, cold wall temperature, and fluid temperature are assumed to be uniform throughout a panel. The coolant channel dimensions and wall temperatures are allowed to vary from station to station. The flow conditions are assumed to be identical for all channels at a given nozzle station.

The hot wall heat flux at each axial station is calculated using a modified Bartz [10] correlation. This correlation was identified in [11], which describes a similar regenerative cooling model.

$$\dot{q}_{walls} = h_g * (T_g - T_{hw}) = \frac{k_{lig}}{t_{lig}} * (T_{hw} - T_{cw}) \qquad \textit{Eqn 18}$$

$$h_g = \frac{k_g}{D_{hyd,g}} * 0.026 * Re_g^{0.8} Pr_g^{0.4} * \left(\frac{\rho_g + \rho_{g,hw}}{2\rho_{g,0}}\right)^{0.8} * \left(\frac{\mu_g + \mu_{g,hw}}{2\mu_{g,0}}\right)^{0.2} \qquad \textit{Eqn 19}$$

Where:

$Subscript\ g$	= Exhaust gas
$Subscript\ 0$	= Stagnation properties
D_{hyd}	= Hydraulic diameter
k	= Thermal conductivity
Re	= Reynolds number
Pr	= Prandtl number
ρ	= Density
μ	= Dynamic viscosity

The resulting heat load is used to calculate the net exhaust heat loss as the flow marches from station to station. Exhaust viscosity, thermal conductivity, and specific heat are calculated using CEA. Exhaust density is calculated assuming an ideal gas. The Mach number, static pressure, and static temperature are calculated at each station from the nozzle area ratio and stagnation conditions. The stagnation conditions

are updated as the flow marches along using a quasi-1-dimensional frictionless flow model (Eqn 20 and Eqn 21). A flowchart of the exhaust calculation is provided in Figure 19.

$$\Delta T_{g,0} = \frac{\dot{Q}_{walls}}{\dot{m}_g c_{p,g}} \qquad \textit{Eqn 20}$$

$$\Delta P_{g,0} = -P_{g,0} * \frac{\gamma M^2 * \Delta T_{g,0}}{2T_{g,0}} \qquad \textit{Eqn 21}$$

Where:
M = Mach number
c_p = Specific heat

The exhaust calculation produces the wall heat flux as a function of axial position in the combustion chamber and nozzle. When simulating a conventional propulsion system, the exhaust calculation only needs to be performed once for the steady-state chamber conditions. When simulating an RDRE, the time dependent nature of the exhaust flow must be accounted for. The RDRE performance code discussed previously is used to calculate the time dependent RDRE chamber conditions. The exhaust marching calculation is repeated at each time step to calculate wall heat flux as a function of both axial position and time. The RDRE performance code includes its own heat transfer correlation. An iterative procedure scales this heat transfer correlation until the time-averaged heat load simulated by the performance code matches the time-averaged heat load calculated by the exhaust marching calculation, thus closing conservation of energy between the two models. A flowchart of this solution process is provided in Figure 8.

The cold wall heat flux adsorbed by each trapezoidal panel is calculated using a Sieder-Tate [12] correlation (Eqn 23). The channel ribs are treated as finned heat transfer surfaces with adiabatic tips (Eqn 24). The closeout wall is treated as adiabatic.

$$\dot{q}_{walls} A_{trap} = \frac{k_{lig}}{t_{lig}} * (T_{hw} - T_{cw}) = h_c A_{lig} (T_{cw} - T_c) + \dot{Q}_{fin} \qquad \textit{Eqn 22}$$

$$h_c = \frac{k_g}{D_{hyd,c}} 0.027 * Re_c^{0.8} Pr_c^{\frac{1}{3}} * \left(\frac{\mu_c}{\mu_{cw}}\right)^{0.14} \qquad \textit{Eqn 23}$$

$$\dot{Q}_{fin} = \tanh\left(H_{fin} * \sqrt{\frac{2h_c}{k_{lig} t_{rib}}}\right) * L_{trap} * \sqrt{2h_c t_{rib}} * (T_{cw} - T_c) \qquad \textit{Eqn 24}$$

Where:
$Subscript\ c$ = Coolant
A_{trap} = Area of trapezoidal panel being evaluated
L_{trap} = Length of trapezoidal panel being evaluated
A_{lig} = Area of cold wall ligament

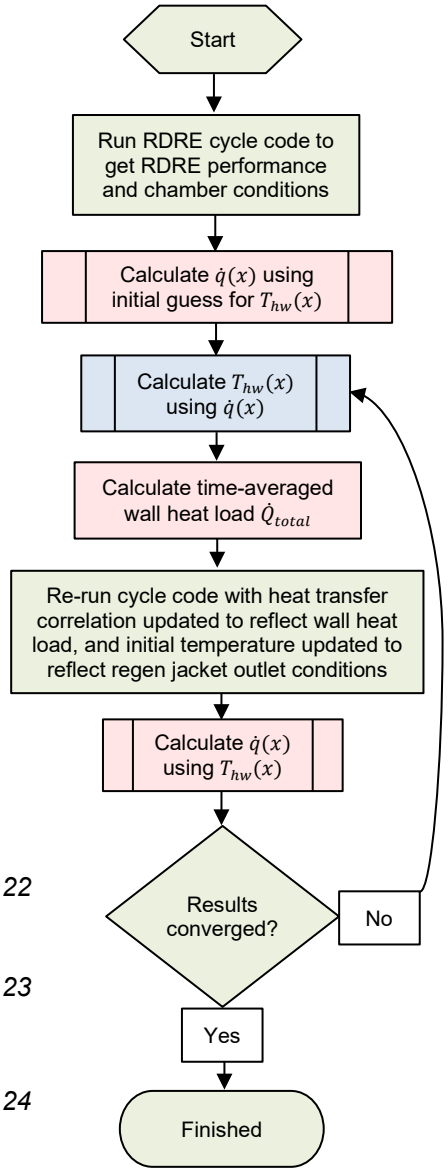

Figure 8: Flowchart of regenerative cooling model solution process. Further information is provided in Figure 19 and Figure 20 in the appendix.

The resulting heat load is used to calculate the coolant temperature rise across each panel. The coolant pressure drop across each panel is calculated using the Darcy-Weisbach equation. The coolant temperature and pressure are updated accordingly from station to station as the flow marches along the cooling channel.

Cooling channel dimensions are optimized at each station. The number of channels (as measured at the throat) is a user input. The maximum allowable channel depth, minimum allowable rib thickness, minimum allowable channel width, and maximum allowable hot wall temperature are user inputs. For RDRE models, if more inner body channels are input than can fit in the aerospike, the jacket is bifurcated at the necessary location. The aerospike is truncated to 50% of its length to reduce the inner body wall area. Prior work on RDRE nozzles indicates that the truncation's effect on engine performance can be neglected [13]. The model selects the cooling channel dimensions based on three criteria, listed in order of priority. First, the hot wall temperature cannot exceed the user input. Second, the channel aspect ratio – the channel depth over the channel width – is maximized for heat transfer efficiency. Third, the channel flow area is maximized to reduce the pressure drop. If a single commodity is used as coolant, the mass flow rate ratio for the outer vs. inner body is set according to the heat load ratio. A flowchart of the coolant calculation is provided in Figure 20.

The regenerative cooling jacket model is critical to the MIURA-1 trade study. Given this, a significant model validation effort was performed using the RL-10 rocket engine as a benchmark. The RL-10 regenerative cooling jacket dimensions and engine operating conditions were input to the model. To simulate conventional rocket engines, CEA is used in place of the RDRE cycle code within the regen model. The model's predicted jacket temperature rise, jacket pressure loss, and exhaust specific impulse were compared to test data from hotfires conducted without the passively cooled nozzle extension [14]. The results show excellent agreement in Table 17, Figure 21, and Figure 22.

GRCop-42 is used for the regen cooling jacket material due to its high thermal conductivity at high temperatures [16]. This limits the maximum hot wall temperature to 1800 °R. The minimum channel dimensions are limited to 0.010" based on the authors' experience with minimum-size chemically etched cooling channels. The regen cooling jacket model settings for the MIURA-1 trade study are listed in Table 14.

Table 11: Baseline TEPREL-B performance and mass calculation

Parameter	Value
Combustion efficiency	91% (assumed)
Specific impulse	240.0 sec
Coolant flow rate	8.4 lbm/sec
Number of channels	100 (assumed)
Jacket pressure drop	4 psid
Jacket temperature rise	570 °R
Nozzle area ratio	4 (assumed)
Exhaust exit pressure	14.7 psia
Jacket mass	93 lbm

MASS ESTIMATE MODEL

The regenerative cooling jacket mass is calculated from the geometry shown in Figure 7. The regen cooling model breaks the engine geometry into flat panels and outputs the full regen jacket geometry. This makes calculating the jacket mass simple. The closeout is assumed to be quarter inch thick stainless steel and is included in the jacket mass calculation. The regenerative cooling jacket model was run for the TEPREL-B rocket engine using the public information in Table 9. To match the cited TEPREL-B specific

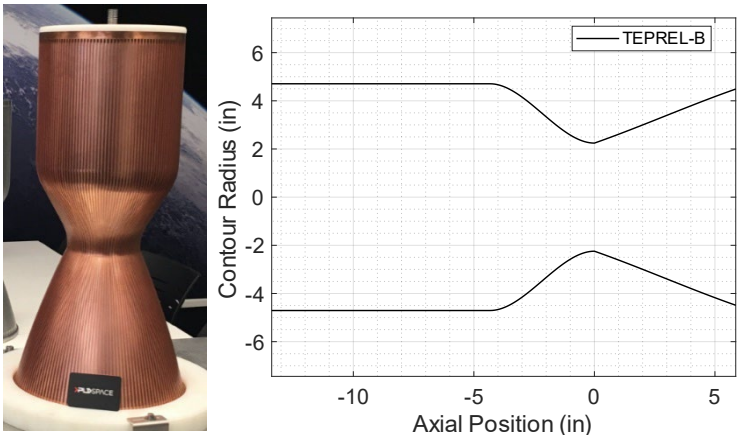

Figure 9: The TEPREL-B regen cooling jacket with closeout removed [20] (left) alongside the TEPREL-B geometry model used for the MIURA-1 trade study (right).

impulse, the combustion efficiency is assumed to be 91%. The settings listed in Table 14 were used for the TEPREL-B calculation. These are the settings used for the RDRE calculations, and so they are used for the TEPREL-B calculation to allow good comparison between the results. Note that these settings produce cooling channels that are likely thinner and have a higher aspect ratio than the true TEPREL-B cooling channels. The results of the TEPREL-B calculation agree with the public information and are shown in Table 11. The calculated TEPREL-B jacket mass is 93 lbm. The modeled geometry is shown in Figure 9. The TEPREL-B mass is not publicly available for anchoring this calculation. However, it agrees well with the mass of the SpaceX Kestrel rocket engine, a 114 lbm pressure-fed kerolox engine in the same thrust class [18].

The propellant tank wall thickness is calculated using the simple hoop stress formula for thin-walled cylindrical pressure vessels [8]. The propellant tanks are modeled as cylindrical with hemisphere endcaps. A scaling law is used to calculate the required propellant tank volume in Eqn 25 (fuel) and Eqn 26 (oxidizer). The propellant tank mass is estimated using Eqn 28. The propellant tank mass was estimated for the baseline MIURA-1 design using the public information in Table 9. The calculation is shown in Table 12.

$$V_{prop,fu} = m_{prop,fu} * \frac{600[L]}{1{,}030[lbm]} \quad \textit{Eqn 25}$$

$$V_{prop,ox} = m_{prop,fu} * \frac{1000[L]}{2{,}420[lbm]} \quad \textit{Eqn 26}$$

$$H_{prop} = \frac{V_{prop}}{\pi r^2} - \frac{4}{3}r \quad \textit{Eqn 27}$$

$$m_{tank} = \pi\rho\left(H_{cyl} * ((r+t)^2 - r^2) + \frac{4}{3}((r+t)^3 - r^3)\right) \quad \textit{Eqn 28}$$

Where:

H_{prop} = Height of propellant tank barrel
V_{prop} = Volume of propellant held by tank
ν_{ullage} = Ullage volume fraction (4% for MIURA-1)
r = Tank inner radius (13.8” for MIURA-1)
t = Tank wall thickness
ρ = Tank wall density

Table 12: Baseline MIURA-1 propellant tank mass calculation

Parameter	Value
Wall material	Aluminum 6061-T6
Wall yield strength [17]	39 ksi
Wall density [17]	174 lbm/ft^3
Safety factor	1.5
Calculated fuel tank mass	126 lbm
Calculated oxid tank mass	270 lbm

Table 13: Baseline MIURA-1 pressurant mass calculation

Parameter	Value
Wall material	T800-H Carbon Fiber Composite
Wall yield strength [19]	424 ksi
Wall density [19]	113 lbm/ft^3
Safety factor	1.5
Calculated COPV mass	58 lbm
Helium density	3.54 lbm/ft^3
Calculated helium mass	33 lbm

The helium COPV mass is calculated using the same method as the propellant tanks. The helium COPV is a carbon fiber overwrap with an aluminum liner. The aluminum liner is neglected. The COPV geometry is cylindrical with hemisphere endcaps. The initial COPV pressure and temperature is held constant at 6,000 psia, 68 °F. The tank volume is changed to vary the amount of helium in the tank. A scaling law is used to calculate the required COPV volume in Eqn 29. The total pressurant mass – including helium gas and COPV wall – is estimated using Eqn 28. The helium COPV and helium gas mass were estimated for the baseline MIURA-1. The calculation is shown in Table 13.

$$V_{COPV} = 260[L] * \left(\frac{P_{fuel} * V_{fuel} + P_{oxid} * V_{oxid}}{390[psia] * 600[L] + 520[psia] * 1000[L}\right) \quad \textit{Eqn 29}$$

$$m_{press} = V_{COPV}\rho_{GHe} + \pi\rho_{COPV}\left(H_{COPV} * ((r+t)^2 - r^2) + \frac{4}{3}((r+t)^3 - r^3)\right) \quad \textit{Eqn 30}$$

Where:
P = Propellant tank pressures
V = Propellant tank volumes

The gross liftoff mass is estimated using Eqn 31.

$$m_{GLOM} = 1{,}370[lbm] + m_{prop} + m_{tank,fu} + m_{tank,ox} + m_{press} + m_{jacket} + m_{payload} \qquad \textit{Eqn 31}$$

TRAJECTORY MODEL

A simple model was developed for calculating the MIURA-1 trajectory in two dimensions. The trajectory model numerically integrates the velocity and acceleration vectors. The vehicle mass is numerically integrated assuming engine propellant consumption is constant. The forces due to gravity, thrust, and atmospheric drag are accounted for. The engine thrust is calculated using Eqn 32, which compensates for the performance increase at higher altitudes.

$$F = \dot{m}_e g I_{sp,SL} + (P_e - P_{amb})A_e \qquad \textit{Eqn 32}$$

Where:
$I_{sp,SL}$ = Sea-level specific impulse
P_{amb} = Local ambient pressure
A_e = Nozzle exit area

Curves for atmospheric pressure and density are provided in the appendix (Figure 23 and Figure 24). The MIURA-1 drag coefficient is assumed to be 0.35. The trajectory model is validated by comparing its baseline MIURA-1 performance predictions to those cited in the payload user's manual [4]. The results in Figure 10 show acceptable agreement.

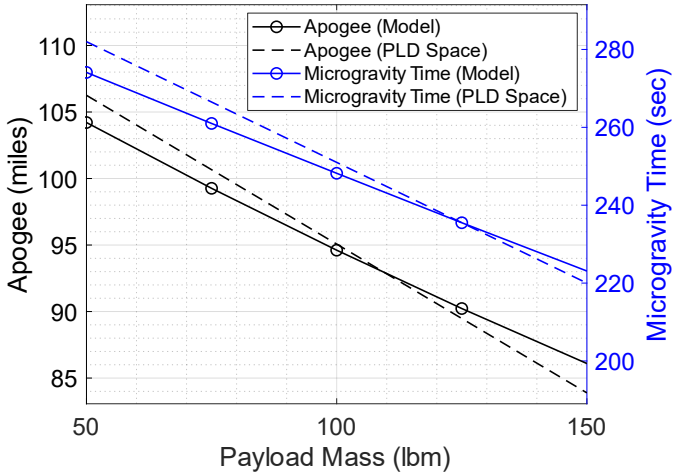

Figure 10: Trajectory model validation against cited MIURA-1 performance data [4]

REGENERATIVE COOLING ANALYSIS

It should be noted that the results of the MIURA-1 trade study are highly dependent on the heat transfer calculations. The regenerative cooling jacket model's predictions were validated using a conventional rocket model compared to RL-10 experimental data. Ideally, the RDRE model would be compared to experimental data as well. Both models use the same heat transfer correlations. However, experimental data for RDRE heat transfer is sparse. Therefore, there is significant uncertainty in the RDRE heat transfer calculations. The regen cooling jacket model settings for the MIURA-1 trade study are listed in Table 14.

Table 14: Regen cooling jacket model settings for MIURA-1 trade study

Parameter	Assumed Value
Max allowable hot wall temperature	1,800 °R
Min allowable rib thickness	0.010"
Min allowable channel width	0.010"
Max allowable channel depth	0.500"
Max allowable kerosene temperature	1,100 °R
Ligament thickness	0.030"
Ligament thermal conductivity	330 W/m-K
Channel wall roughness	1 μm
Kerosene inlet temperature	430 °R
Oxygen inlet temperature	166 °R
Jacket material	GRCop-42
Jacket density	549 lbm/ft^3
Closeout material	Stainless Steel
Closeout density	490 lbm/ft^3

For regenerative cooling schemes using kerosene, coking must be considered. For this study, the kerosene coolant is not allowed to exceed a coking limit of 1100 °R [21]. The combustion chamber must be sufficiently short so that the total heat load absorbed by the kerosene coolant does not result in a jacket outlet temperature exceeding 1100 °R. For RDREs, the combustion chamber should also respect the effective length limit. The effective length is the chamber length required such that the cycle is complete by the time the detonation wave has traveled around the chamber circumference. Its calculation and physical interpretation are discussed in [7]. In brief it correlates reasonably closely with 1.2-1.5 times the detonation height, where the flow field is almost entirely sonic or supersonic. The required combustion chamber length for an RDRE is a topic of active research; the optimal value is not known. However, it is believed that at minimum, the combustion chamber length cannot be below the effective length.

Using these limits, one can determine the feasibility of a kerosene regeneratively cooled RDRE. The regenerative cooling model and RDRE cycle code were used to run a parametric sweep across a range of hub-to-tip ratios and initial pressures. The mean combustion chamber diameter required to produce 6,800 lbf of thrust was calculated. Then, the required combustion chamber length such that the jacket outlet temperature is below 1100 °R was calculated. The jacket inlet temperature is set to 430 °R; any lower, and kerosene gelling must be considered. Nozzle area ratio was held constant at 5.0. Initial pressures were evaluated from 120 psia to 320 psia. REFPROP was used to generate RP-1 fluid properties [15].

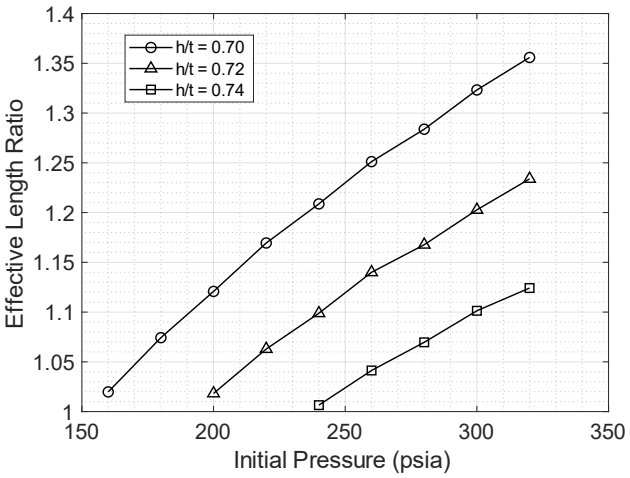

Figure 11: Parameter sweep results for kerosene regeneratively cooled 6,800 pound thrust RDRE effective length ratios. The effective length ratio is the chamber length divided by the effective length.

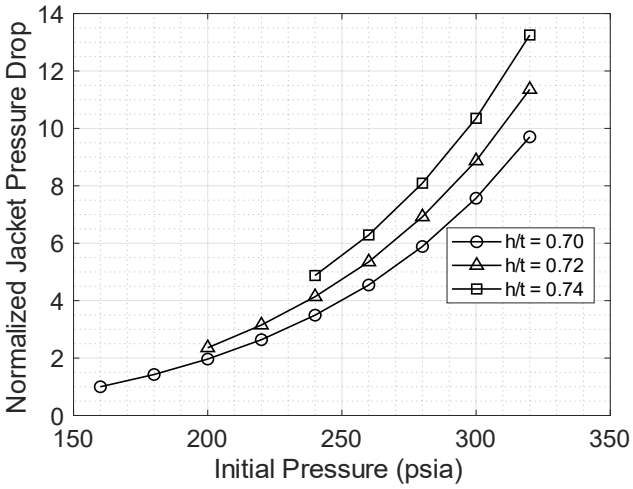

Figure 12: Parameter sweep results for kerosene regeneratively cooled 6,800 pound thrust RDRE regen jacket pressure drop.

The results of the kerosene regeneratively cooled 6,800 pound thrust RDRE parameter sweep in Figure 11 show that hub-to-tip ratios greater than 0.74 are not feasible. Larger hub-to-tip ratios result in chamber lengths shorter than the effective length. Although the results show that kerosene-cooled RDREs can close thermally with chamber lengths greater than the effective length, these chambers are still very short – an effective length ratio of 1 typically corresponds to a chamber aspect ratio of about 1.5. Assuming that an RDRE of this length scale is feasible, a regen jacket was designed for each case. The jacket design is not optimized, and simply uses the maximum possible amount of cooling channels. This enables a qualitative comparison of the jacket pressure drop required to cool each RDRE configuration. The results are normalized to the minimum pressure drop across all cases, for comparison. The results show that as hub-to-tip ratio and initial pressure increase, the jacket pressure drop increases.

The results present a difficult situation for regeneratively cooled kerosene RDREs. The results show that, for a design which closes thermally, a short chamber and a low hub-to-tip ratio are required. [22] provides an overview of experimental liquid bipropellant RDE configurations that have been ran successfully, but the lower limits for these parameters are not known. Figure 11 shows that a longer

chamber can be achieved if the initial RDRE pressure is increased. However, even if the conventional TEPREL-B chamber pressure is used for the initial RDRE pressure, the effective length ratio is still less than 1.5. Additionally, the jacket pressure drop increases with hub-to-tip ratio and initial pressure. These factors suggest that, to increase the chamber length beyond the effective length for a kerosene cooled 6,800 lbf RDRE, the supply pressure required will be too great to make an RDRE trade feasible.

Alternative strategies are available for achieving longer RDRE chambers. The annulus configuration of an RDRE combustion chamber naturally lends itself to using both propellants to cool the chamber. One commodity can be used to cool the inner body, and the other commodity can be used to cool the outer body. By sharing the heat load with the liquid oxygen, the heat absorbed per mass of kerosene is reduced. The feasibility of regenerative cooling using liquid oxygen has been experimentally demonstrated in conventional rocket engines with copper jackets [23]. However, it is noted that these experiments had hot wall temperatures at 900 °R, below the assumed hot wall temperature for this study. If the oxidizer is used to cool the outer body, then the kerosene only needs to cool the inner body and aerospike. Note that dual cooling is not necessary for the conventional TEPREL-B rocket engine since its jacket pressure drop and temperature rise (shown in Table 11) are already acceptably low when using kerosene. Another parametric sweep was run using this cooling scheme. REFPROP was used to generate LOX fluid properties [15]. The results of this dual commodity cooling parameter sweep are shown in Figure 13. The results indicate that using both commodities to cool the chamber results in a 4x increase in the chamber effective length ratio. Hub-to-tip ratios greater than 0.74 become possible. However, if liquid oxygen is used as a coolant, it must be kept above its critical pressure (732 psia). Otherwise, the fluid will boil in the coolant tubes. Running more fuel-rich is another strategy for reducing the heat load on the kerosene. A final parametric sweep found that reducing the mixture ratio to 1.90 results in a 2x increase in the chamber effective length ratio compared to the baseline 2.35 mixture ratio.

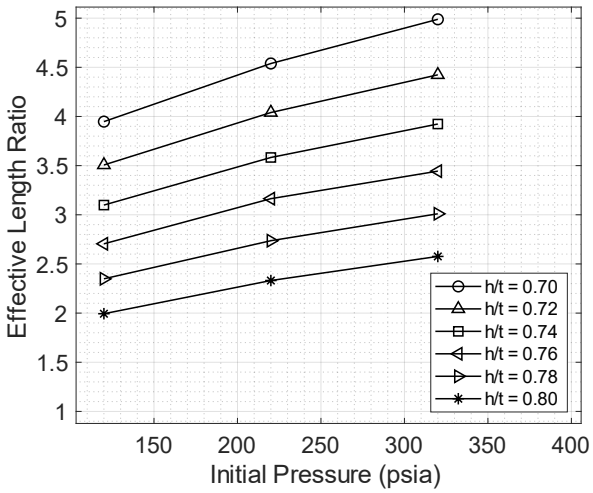

Figure 13: Parameter sweep results for dual commodity cooled 6,800 pound thrust RDRE effective length ratios.

Three cases were selected from the parametric sweeps. The first case uses kerosene cooling only, at a 0.70 hub-to-tip ratio and 160 psia initial pressure. The chamber aspect ratio for this case is 0.6. This is the highest aspect ratio that could be used without violating the coking limit. The 160 psia initial pressure was selected to respect the effective length limit – lower initial pressures were found to require chamber lengths below the effective length (seen in Figure 11). The second case uses dual commodity cooling, at a 0.80 hub-to-tip ratio and 220 psia initial pressure. The chamber aspect ratio for this case is 2.6, which similarly is the largest value that could be used without violating the coking limit. The 220 psia initial pressure was selected because it produces a high specific impulse with a reasonable pressure drop. The third case reduces the mixture ratio to 1.90. This enables the chamber aspect ratio to increase to 5.0 without violating the coking limit. These three cases are used to perform the MIURA-1 RDRE trade. The RDRE geometry for each case is provided in Figure 25, Figure 26, and Figure 27 in the appendix.

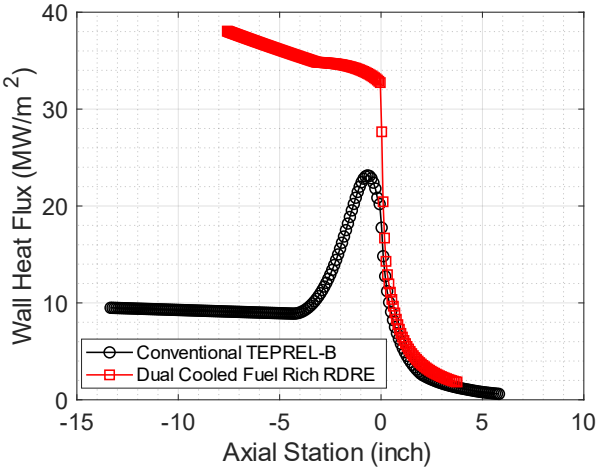

Figure 14: Predicted wall heat fluxes for the conventional TEPREL-B and the dual cooled, fuel rich RDRE

To highlight why RDRE, regenerative cooling has such a significant impact on system performance, Figure 14 shows the model prediction for wall heat fluxes in the conventional TEPREL-B rocket engine, and in the dual cooled fuel rich RDRE. The peak heat flux is typically experienced by conventional rocket engines at the throat, where the flow is sonic. In an RDRE, the flow is sonic or near sonic throughout the entire combustion chamber. Additionally, the chamber temperatures are higher due to the nature of detonative combustion. The result is a peak RDRE wall heat flux about 1.6x greater than the conventional engine's peak wall heat flux, despite the RDRE running more fuel rich. This peak heat flux is spread across the entire combustion chamber for an RDRE, whereas a conventional rocket engine experiences its peak heat flux only in a localized region near the throat. Thus, the cooling channels must absorb a larger amount of heat per wall surface area. This necessitates higher coolant velocities and correspondingly higher coolant pressure drops. Additionally, an RDRE chamber has a larger amount of surface area than a conventional chamber due to the annular detonation channel geometry. This further exacerbates the total heat load that an RDRE regen cooling jacket must handle. The high heat loads lead to performance losses due to wall heat losses. The high pressure drops require higher propellant tank pressures, increasing the propellant tank mass. This is why RDRE regenerative cooling has a significant impact on system performance.

Table 15: Model outputs for three regenerative cooling analysis cases

Parameter	Kerosene Cooling Only		Dual Commodity Cooling		Dual Cooling With Reduced Mixture Ratio	
Thrust	6,800 lbf		6,800 lbf		6,800 lbf	
Initial pressure	160 psia		220 psia		220 psia	
Nozzle area ratio	5		5		5	
Mixture ratio	2.35		2.35		1.90	
Hub-to-tip ratio	0.70		0.8		0.8	
Chamber aspect ratio	0.6		2.6		5.0	
Mean diameter	5.50"		6.60"		6.84"	
Specific impulse	270.7 sec		265.4 sec		252.4 sec	
Wall heat loss as percent of total reaction heat	2.2%		6.5%		8.3%	
Chamber channel width	0.97"		0.73"		0.76"	
Chamber outer diameter	6.47"		7.33"		7.60"	
Chamber inner diameter	4.53"		5.87"		6.08"	
Chamber length	1.16"		3.80"		7.60"	
Detonation frequency	5,860 Hz		4,870 Hz		4,520 Hz	
Jacket mass	27 lbm		42 lbm		74 lbm	
Jacket heat load	2,166 BTU/sec		6,455 BTU/sec		8,040 BTU/sec	
Initial temperature	609 °R		958 °R		1,059 °R	
	Inner	**Outer**	**Inner**	**Outer**	**Inner**	**Outer**
Coolant	Kerosene	Kerosene	Kerosene	LOX	Kerosene	LOX
Coolant flow rate	2.8 lbm/s	4.7 lbm/s	7.7 lbm/s	18.1 lbm/s	9.3 lbm/s	17.6 lbm/s
Number of channels	724	826	920	772	954	800
Inlet temperature	430 °R	430 °R	430 °R	166 °R	430 °R	166 °R
Outlet temperature	1,043 °R	1,093 °R	1,093 °R	776 °R	1,085 °R	1,005 °R
Jacket temperature rise	613 °R	663 °R	663 °R	619 °R	655 °R	839 °R
Inlet pressure	780 psia	780 psia	358 psia	885 psia	306 psia	815 psia
Outlet pressure	296 psia	232 psia	293 psia	738 psia	290 psia	735 psia
Jacket pressure drop	484 psid	550 psid	65 psid	147 psid	16 psid	80 psid

MIURA-1 TRADE STUDY RESULTS

A parametric sweep was run on chamber pressure for the conventionally powered MIURA-1. This sweep sought to identify if the performance of the MIURA-1 system could be enhanced by increasing propellant tank pressure, thereby increasing the chamber pressure. This is similar to the optimization that was performed on the conventionally powered L-MAV. The optimal throat diameter and expansion ratio was solved for at each chamber pressure. The sweep found that the system-level impacts of increasing the TEPREL-B chamber pressure result in reduced apogee and microgravity time if gross liftoff mass is held fixed. Therefore, since the baseline MIURA-1 already represents the optimal configuration, the RDRE configuration is compared to the baseline configuration. Figure 10 shows the trajectory model output for the conventional MIURA-1. For good comparison, the model outputs for the RDRE MIURA-1 are compared to these model outputs for the conventional MIURA-1.

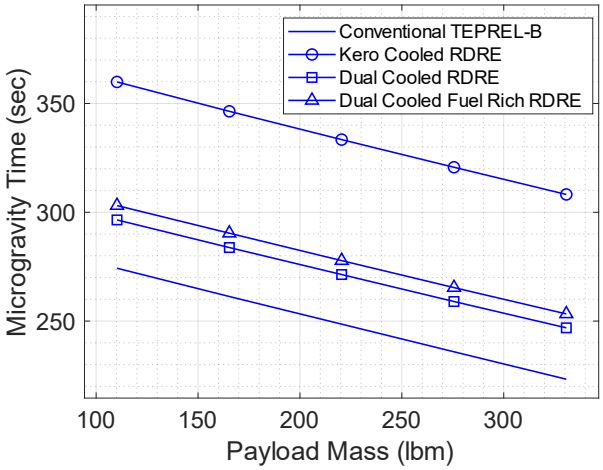

Figure 15: Predicted microgravity time for each MIURA-1 configuration. Total vehicle mass (excluding payload) is 5,400 lbm for all cases.

The predicted microgravity time for each MIURA-1 configuration is shown in Figure 15. **All RDRE configurations achieve higher performance than the baseline.** Figure 16 also shows the predicted apogee for each MIURA-1 configuration. Higher propellant tank pressures are required when using an RDRE due to the regen jacket pressure drop. Despite this, there is a net performance gain from using an RDRE on this vehicle. These performance predictions were generated holding vehicle mass constant at 5,400 lbm for all cases to compare performance. An alternate comparison can be drawn by holding the payload mass constant at 220 lbm. The apogee is held constant at 94.7 miles – this is the predicted apogee for the baseline MIURA-1 configuration. The total vehicle mass is allowed to vary to achieve this apogee. This enables comparison of the vehicle size required for each configuration to achieve a reference mission. The results for this reference mission are shown in Table 16.

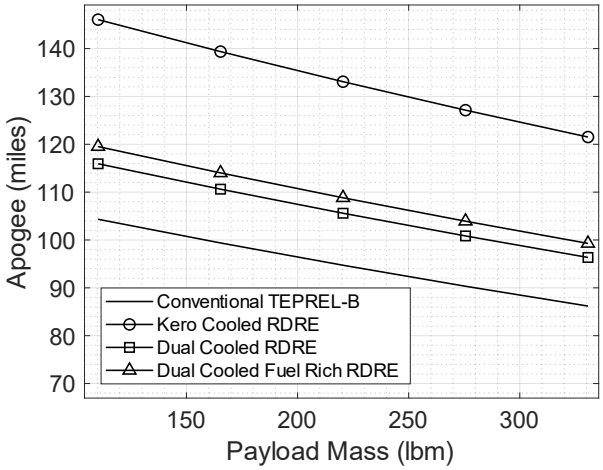

Figure 16: Predicted apogee for each MIURA-1 configuration. Total vehicle mass (excluding payload) is 5,400 lbm for all cases.

There is uncertainty in the optimal hub-to-tip ratio and chamber aspect ratio for an RDRE; this is why multiple RDRE configurations were examined. Of the three RDRE configurations examined, the dual cooled fuel rich RDRE is the most conservative (in terms of wall heat loss) because it uses the largest hub-to-tip ratio and chamber aspect ratio. Large hub-to-tip ratios correspond to smaller detonation channel widths. Large aspect ratios correspond to longer chambers for a given mean diameter. Both of these factors increase the amount of wall heat loss for a given thrust class, and therefore the most conservative case is the one with the largest hub-to-tip ratio and largest chamber aspect ratio. If vehicle mass is held constant at the 5,400 lbm baseline, then the dual cooled fuel rich RDRE MIURA-1 can achieve 12% more microgravity time than the baseline. If the payload mass is held constant at 220 lbm, then the dual cooled fuel rich RDRE MIURA-1 can be 8% shorter and 11% lighter than the baseline.

Table 16: Vehicle length and mass reductions achieved by different MIURA-1 RDRE configurations for a reference mission. The reference payload is 220 lbm, and the reference apogee is 97.4 miles.

Component	Conventional TEPREL-B	Kero Cooled RDRE	Dual Cooled RDRE	Dual Cooled Fuel Rich RDRE
COPV barrel length	15.5”	11.3”	22.5”	15.6”
Fuel barrel length	56.5”	33.7”	43.9”	53.5”
Oxid barrel length	107.2”	65.6”	89.2”	81.6”
Engine length	19.0”	8.4”	8.6”	8.9”
Total vehicle length	500.0”	420.8”	466.0”	461.4”
Length reduction	N/A	-15.8%	-6.8%	-7.7%
Fuel tank pressure	390 psia	780 psia	360 psia	310 psia
Oxid tank pressure	520 psia	520 psia	890 psia	740 psia
Fuel tank mass	126 lbm	179 lbm	98 lbm	96 lbm
Oxid tank mass	270 lbm	185 lbm	396 lbm	309 lbm
Pressurant mass	91 lbm	80 lbm	107 lbm	91 lbm
Jacket mass	93 lbm	27 lbm	42 lbm	74 lbm
Usable propellant	3,450 lbm	2,290 lbm	2,857 lbm	2,878 lbm
Total vehicle mass (excluding payload)	5,400 lbm	4,131 lbm	4,871 lbm	4,818 lbm
Mass reduction	N/A	-23.5%	-9.8%	-10.8%

SUMMARY AND CONCLUSIONS

A system trade was presented which analyzed the vehicle-level impact of including a Rotating Detonation Rocket Engine (RDRE) as the propulsion for the Mars Sample Return Campaign (MSRC) Liquid Mars Ascent Vehicle (L-MAV). This trade focused on potential reductions in overall vehicle mass enabled by using an RDRE. The results showed that a L-MAV optimized to use an RDRE achieved a gross liftoff mass of 591 lbm. A similar analysis showed that a L-MAV optimized to use a conventional rocket engine achieved a gross liftoff mass of 643 lbm. Therefore, the use of an RDRE resulted in an an 8.1% mass reduction. This suggests there is a tangible system-level benefit to using an RDRE for highly mass-constrained, in-space applications in the 300 to 1,500 lbf thrust class. The primary benefit identified for in-space applications is the reduced propellant tank pressure enabled by pressure gain combustion.

An additional system trade was presented which analyzed the vehicle-level impact of including an RDRE as the propulsion for the MIURA-1 sounding rocket. This trade focused on the implications of regeneratively cooling a 6,800 lbf kerolox RDRE. The results showed that RDRE regenerative cooling jackets experience high heat loads and high jacket pressure drops relative to a conventional rocket engine in the same thrust class. These issues can be mitigated by using both propellants for regenerative cooling, and by running more fuel rich. The results of the MIURA-1 trade showed that, holding total vehicle mass constant, an RDRE powered sounding rocket could achieve 12% more microgravity time than a conventionally powered sounding rocket. Alternately, holding payload mass and target apogee constant, an RDRE powered sounding rocket can be 8% shorter and 11% lighter than a conventional sounding rocket. These results suggest there is a tangible system-level benefit to using an RDRE for terrestrial applications in the 6,800 lbf thrust class. The primary benefit identified for terrestrial applications is the increased specific impulse enabled by pressure gain combustion.

FUTURE WORK

This work is planned to continue with further vehicle trade studies. The next vehicle trade study is tentatively planned to focus on turbopump-fed methalox systems.

ACKNOWLEDGMENTS

The authors thank Arland Zatania Lojo for his work pulling together public information on the MIURA-1 vehicle. The authors thank Nathan Ballintyn for sharing his test cell experience with rotating detonation engines, and for recommending an assessment of dual commodity cooling.

REFERENCES

1. Perkins, H. D. and Paxson, D.E., ***Summary of Pressure Gain Combustion Research at NASA***, NASA/TM-2018-219874, Glenn Research Center, OH (Apr 2018)

2. Teasley, T.W., Fedotowsky, T.M., Gradl, P.R., Austin, B.L., and Heister, S.D., ***Current State of NASA Continuously Rotating Detonation Cycle Engine Development***, AIAA SciTech Forum, MD (Jan 2023)

3. Oleson, S.R., McGuire, M.L., Sandifer, C.E., ***Mars Sample Return Mission Liquid Mars Ascent Vehicle (MAV) Concept Design***, CD-2011-62, Collaborative Modeling for Parametric Assessment of Space Systems, NASA Internal Document (June 2011)

4. ***MIURA 1 – Payload User's Guide***, Payload Aerospace S.L. (Nov 2018) https://www.pldspace.com/images/MIURA_1/MIURA1_Payload_Users_Guide.pdf

5. Rao, G.V.R., ***Exhaust Nozzle Contour for Optimum Thrust***, Journal of Jet Propulsion, Vol. 28, Iss. 6, (Jun 1958)

6. McBride, B.J. and Gordon, S., ***Computer Program for Calculation of Complex Chemical Equilibrium Compositions and Applications***, NASA-RP-1311, Lewis Research Center, OH (Jun 1996)

7. Paxson, D.E. and Perkins, H.D., ***A Simple Model for Rotating Detonation Rocket Engine Sizing and Performance Estimates***, AIAA SciTech Forum, Virtual Event (Jan 2021)

8. Young, W.C. and Budynas, R.G., ***Roark's Formulas for Stress and Strain, Seventh Edition***, McGraw-Hill (2002)

9. ***Niobium C-103 Alloy for Space Exploration***, Materion (Dec 2022) https://materion.com/-/media/files/alloy/datasheets/other-alloy-products/niobium-c103-alloy-for-space-data-sheet.pdf (retrieved Mar 2024)

10. Bartz, D.R., ***A Simple Equation for Rapid Estimation of Rocket Nozzle Convective Heat Transfer Coefficients***, Journal of Jet Propulsion, Technical Notes (Jan 1957)

11. Schuff, R., Maier, M., Sindiy, O., Ulrich, C, and Fugger, S., ***Integrated Modeling and Analysis for a LOX/Methane Expander Cycle Engine: Focusing on Regenerative Cooling Jacket Design***, 42nd AIAA/ASME/SAE/ASEE Joint Propulsion Conference & Exhibit, CA (July 2006)

12. Sieder, E.N., Tate, G.E., ***Heat Transfer and Pressure Drop of Liquids in Tubes***, Industrial and Engineering Chemistry, Vol. 28, Iss. 12 (Dec 1936)

13. Paxson, D.E., Miki, K., Perkins, H.D., and Yungster, S., ***Computational Fluid Dynamic Optimization of an Experimental Rotating Detonation Rocket Engine Nozzle***, AIAA AVIATION 2022 Forum, IL (Jul 2022)

14. ***Design, Fabrication, and Test of the RL-10 Derivative II Chamber/Primary Nozzle***, NASA CR-179595, Pratt & Whitney, FL (Apr 1989)

15. Lemmon, E.W., Bell, I.H., Huber, M.L., McLinden, M.O., ***NIST Standard Reference Database 23: Reference Fluid Thermodynamic and Transport Properties – REFPROP, Version 10.0***, National Institute of Standards and Technology, Standard Reference Data Program, MD (2018)

16. Minneci, R.P., Lass, E.A., Bunn, J.R., Choo, H. and Rawn, C.J., ***Copper-based alloys for structural high-heat-flux applications: a review of development, properties, and performance of Cu-rich Cu-Cr-Nb alloys***, International Materials Reviews, UK (Oct 2020)

17. ***6061-T6 Aluminum***, MakeItFrom.com https://www.makeitfrom.com/material-properties/6061-T6-Aluminum/ (retrieved Mar 2024)

18. ***Kestrel***, Encyclopedia Astronautica https://web.archive.org/web/20131216104115/http://www.astronautix.com/engines/kestrel.htm (retrieved Mar 2024)

19. ***T800H Intermediate Modulus Carbon Fiber Technical Data Sheet***, Toray Composite Materials America Inc. (Apr 2018) https://www.toraycma.com/wp-content/uploads/T800H-Technical-Data-Sheet-1.pdf.pdf (retrieved Mar 2024)

20. ***TEPREL-B Photo***, PLD Space Twitter (Jul 2017) https://twitter.com/pld_space/status/882630152831721473 (retrieved Mar 2024)

21. Roback, R., Szetela, E.J., and Spadaccini, L.J., ***Deposit Formation in Hydrocarbon Rocket Fuels,*** NASA CR-165405, United Technologies Research Center, CT (Aug 1981)

22. Ballintyn, N.D., Harroun, A.J., and Heister, S.D., ***Current Status of Liquid Bipropellant Detonation-Based Propulsion Devices***, to appear in Journal of Propulsion & Power (retrieved Mar 2024)

23. Armstrong, E.S., and Schlumberger, J.A., ***Cooling of Rocket Thrust Chambers With Liquid Oxygen***, NASA TM-103146, 26th Joint Propulsion Conference, FL (Jul 1990)

APPENDIX

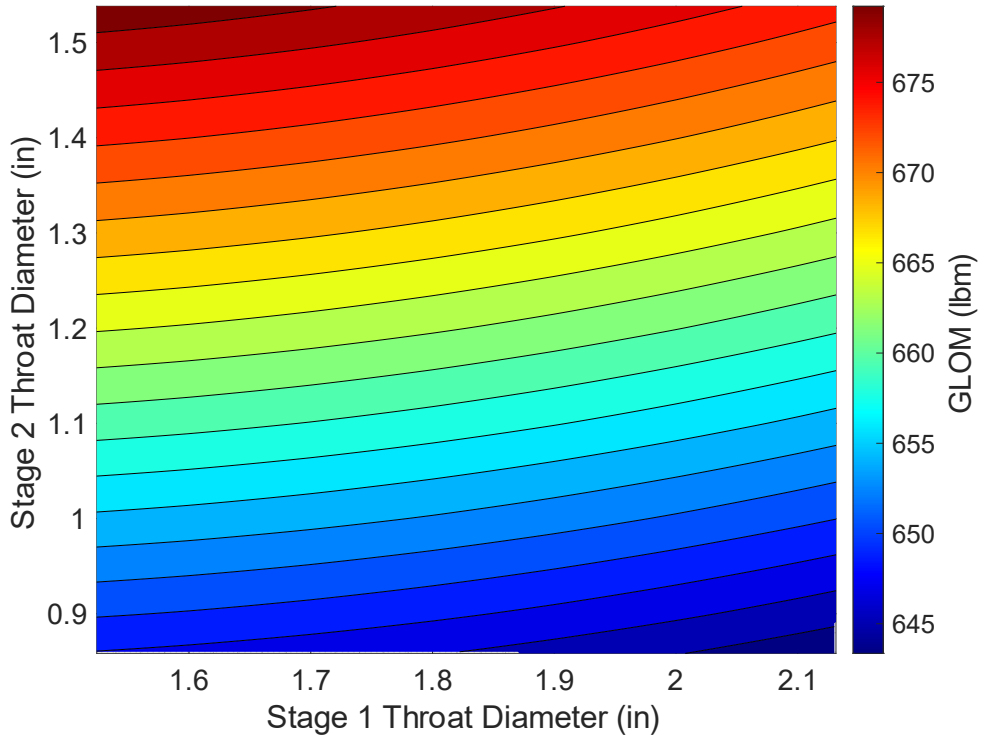

Figure 17: Results of conventional L-MAV optimization for 740 psia tank pressure.

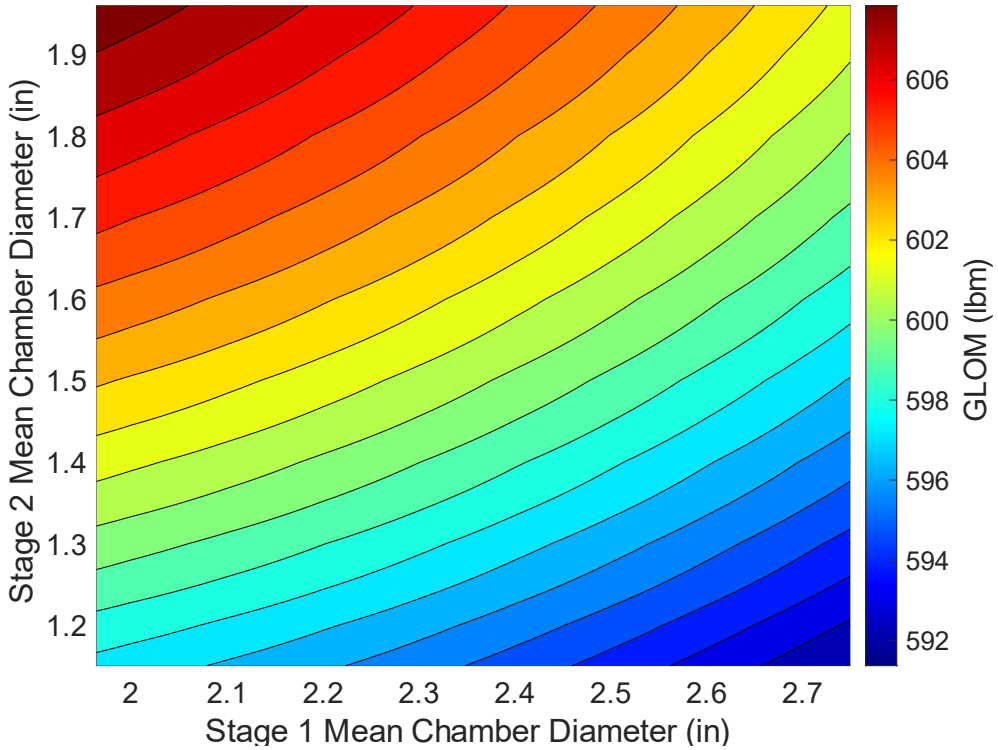

Figure 18: Results of RDRE L-MAV optimization for 680 psia tank pressure.

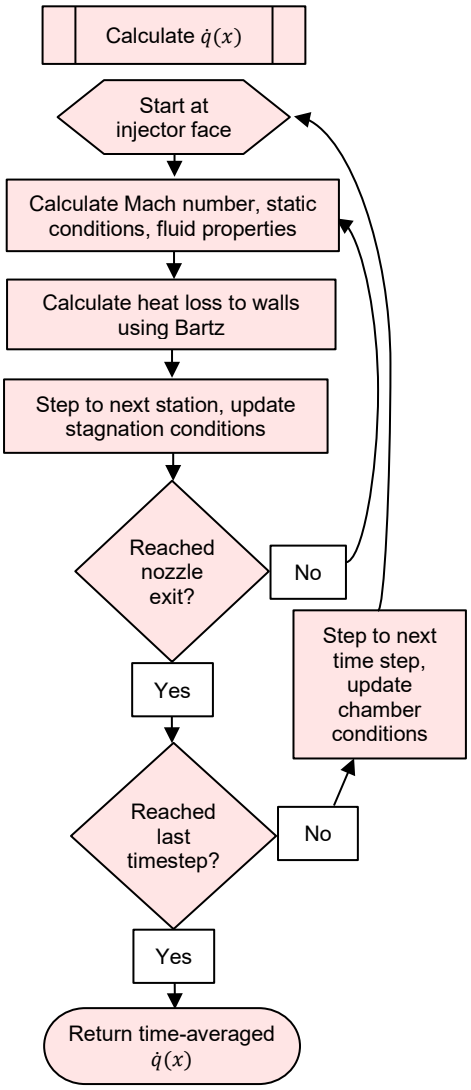

Figure 19: Flowchart of exhaust flow calculation for regenerative cooling model, returning the hot wall heat flux

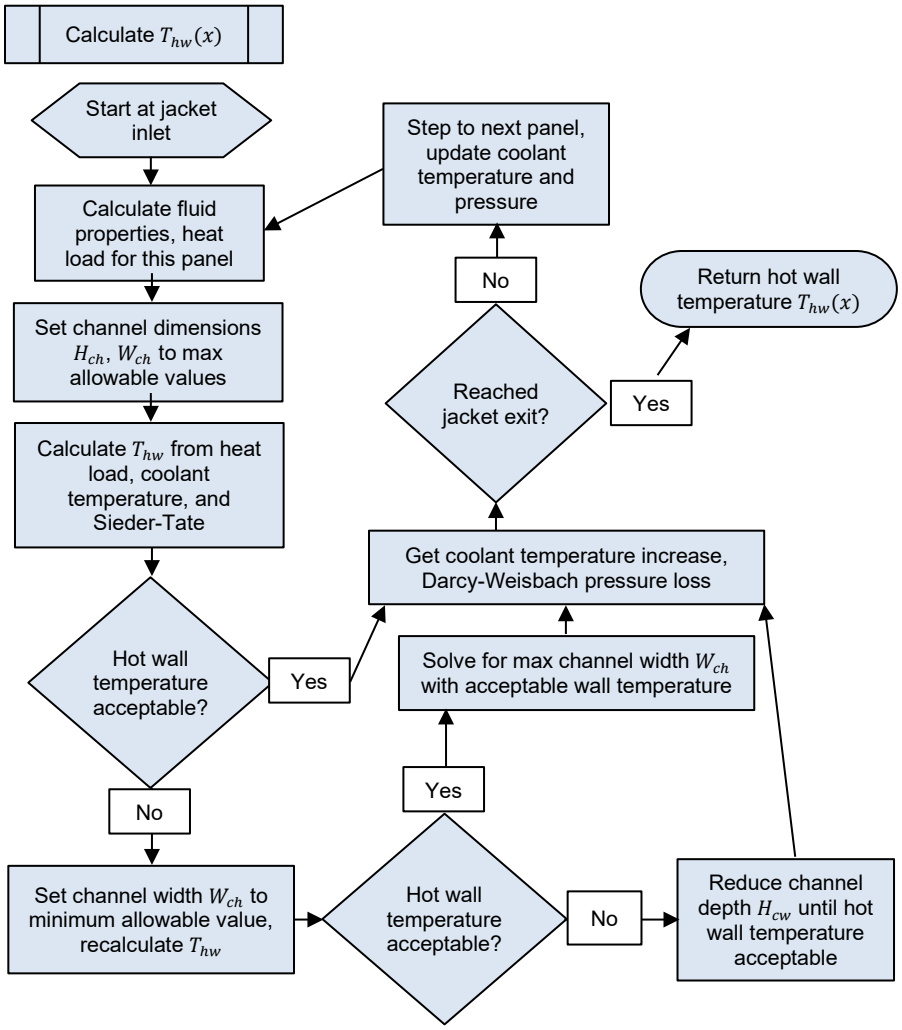

Figure 20: Flowchart of coolant flow calculation for regenerative cooling model, returning the hot wall temperature

Table 17: Regenerative cooling model validation for RL-10. Model predictions are compared to test data shown in [14]

Mixture Ratio	Chamber Pressure	Parameter	Predicted Value	Actual Value [14]	Error
5.00	403 psia	Jacket ΔT	240 °R	300 °R	-60 °R
		Jacket ΔP	154 psia	174 psia	-20 psia
		Specific Impulse	420.0 sec	421.7 sec	-1.7 sec
5.00	443 psia	Jacket ΔT	284 °R	281 °R	+3 °R
		Jacket ΔP	185 psia	183 psia	+2 psia
		Specific Impulse	422.3 sec	423.2 sec	-0.9 psia
6.00	403 psia	Jacket ΔT	337 °R	348 °R	-11 °R
		Jacket ΔP	136 psia	161 psia	-25 psia
		Specific Impulse	407.0 sec	416.9 sec	-9.9 sec
6.00	443 psia	Jacket ΔT	325 °R	332 °R	-7 °R
		Jacket ΔP	162 psia	167 psia	-5 °R
		Specific Impulse	409.3 sec	417.5 sec	-8.2 sec

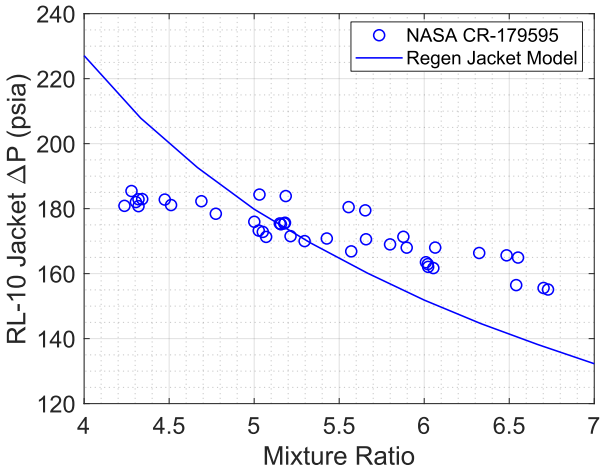

Figure 21: Regen cooling jacket model pressure drop validation against RL-10 test data at 450 psia chamber pressure and varying mixture ratio

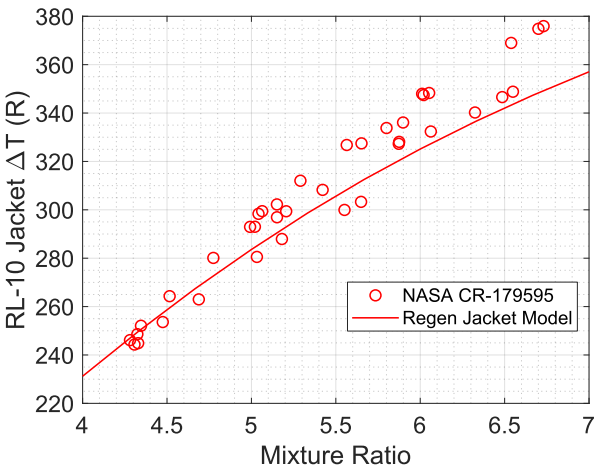

Figure 22: Regen cooling jacket model temperature rise validation against RL-10 test data at 450 psia chamber pressure and varying mixture ratio

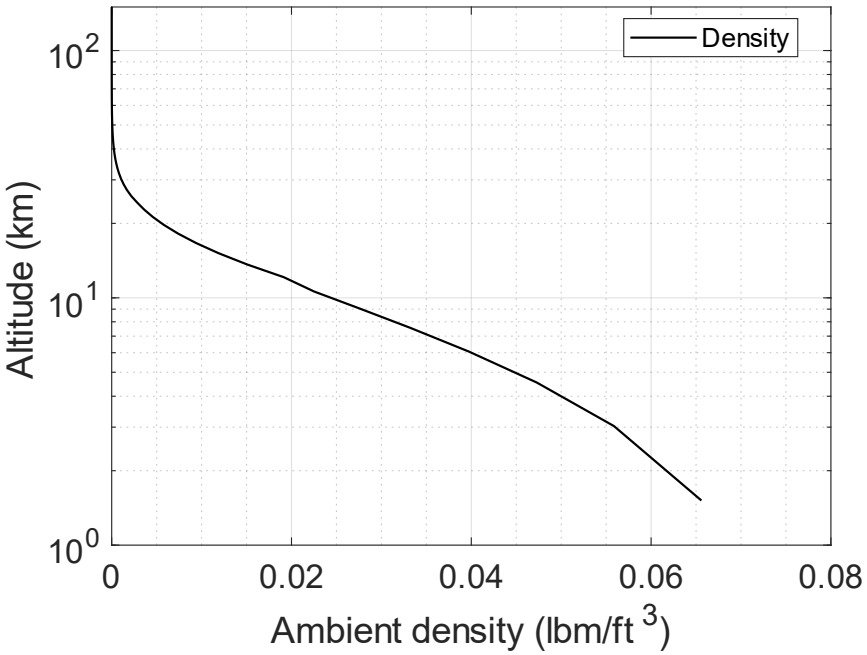

Figure 23: Atmospheric density model

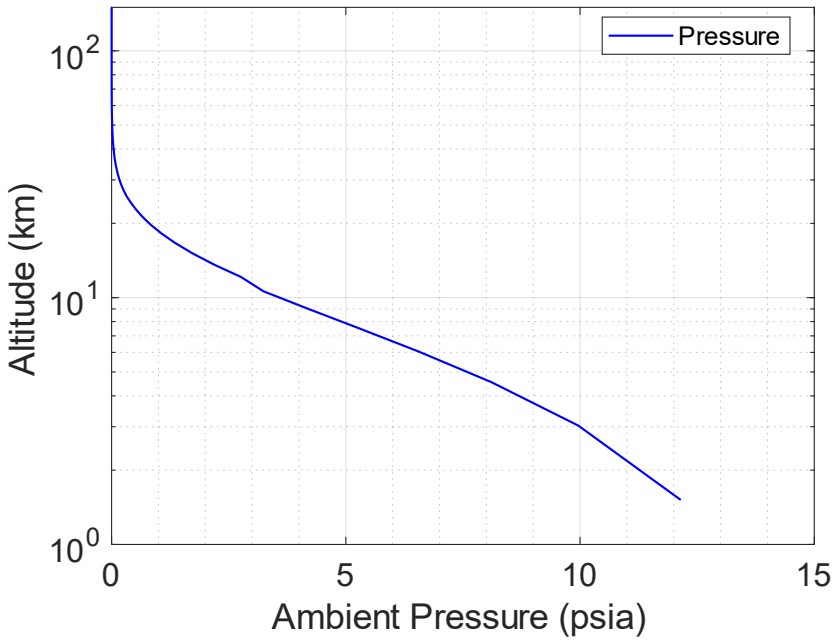

Figure 24: Atmospheric pressure model

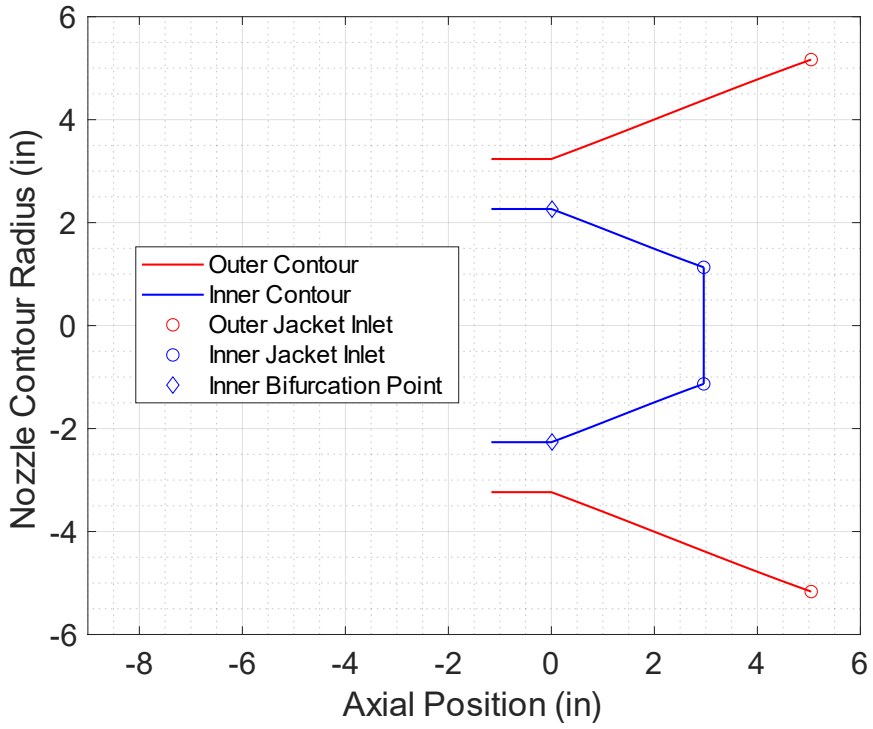

Figure 25: MIURA-1 kerosene cooled RDRE geometry

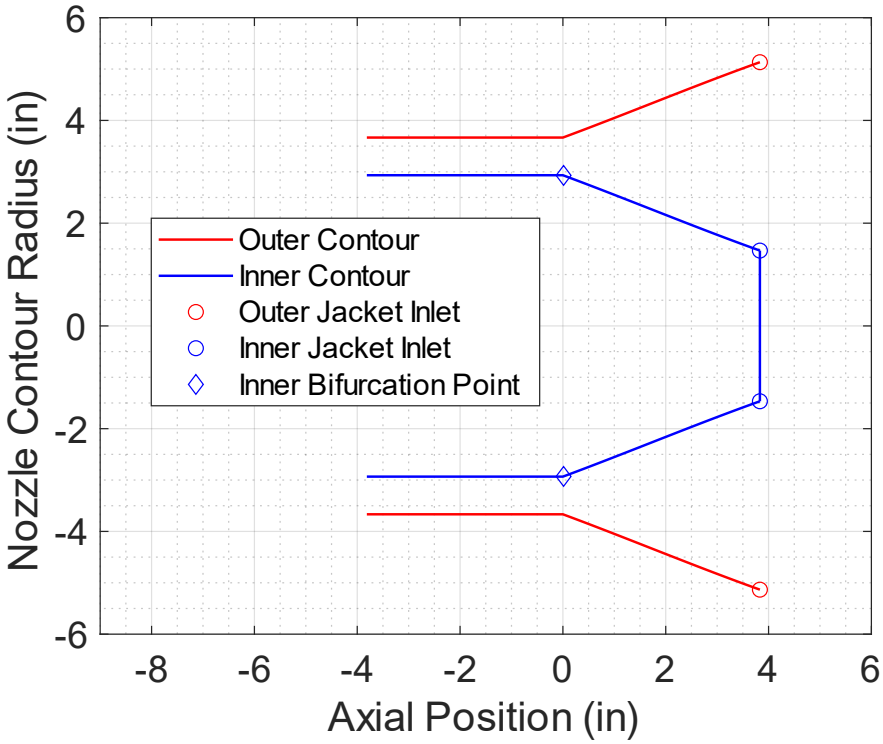

Figure 26: MIURA-1 dual cooled RDRE geometry

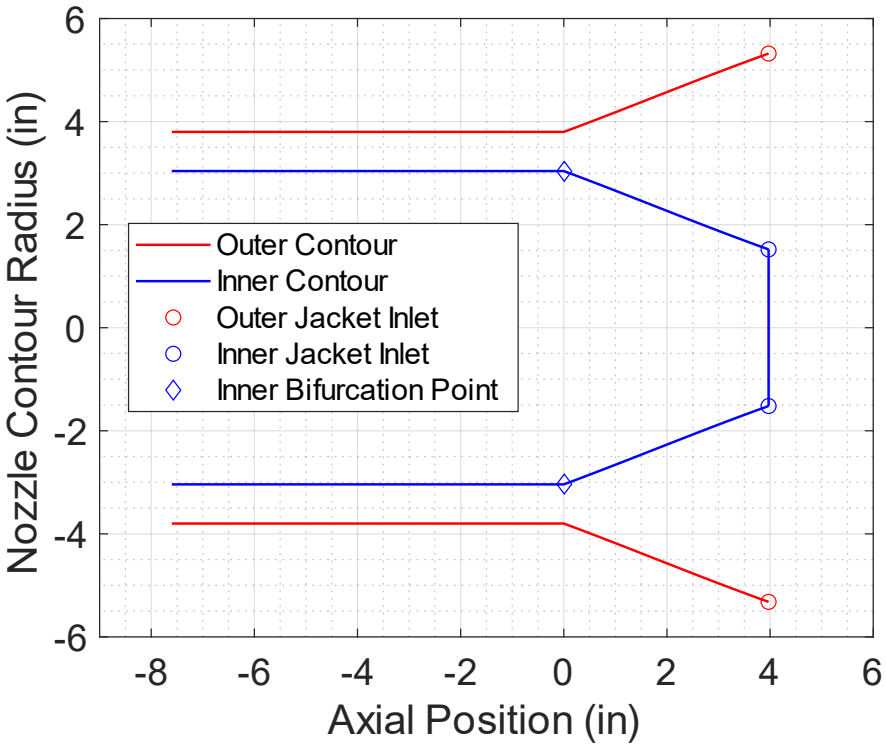

Figure 27: MIURA-1 dual cooled fuel rich RDRE geometry